MU Radar Measurements of Orbital Debris

Toru Sato,* Hidetoshi Kayama,† Akira Furusawa,‡ and Iwane Kimura§
Kyoto University, Kyoto 606, Japan

We have determined distributions of orbital debris vs height and scattering cross section at 46.5 MHz, the lowest frequency ever used for this purpose, from a series of observations made with a high-power VHF Doppler radar (MU radar) of Japan. An automated data processing algorithm has been developed to discriminate echoes of orbiting objects from those of undesired signals such as meteor trail echoes or lightning atmospherics. Although the results are preliminary, they show good agreement with previous results using much higher frequencies.

Nomenclature

$f(\theta)$ = the antenna pattern of the MU radar
G_m = the coefficient of gravity, 3.99×10^{14} m^3/s^2
H = the height of the object, m
P_n' = noise intensity determined from smoothed profile, W
$P_r(t)$ = signal intensity at each time, W
R_e = the Earth's radius, 6.37×10^6 m
t = time, s
t_o = time when the object passes through the center of the main beam, s
v = velocity of the object, m/s
θ = off angle measured from the center of the main beam
σ = standard deviation of noise intensity distribution, W
σ' = standard deviation of signal intensities at each height, W

Introduction

DETERMINATION of mass and shape of orbital debris is an important issue for safe operation of the future space stations. An extensive catalog of orbiting objects provided by the United States Space Command (USSPACECOM) has been the major source of the information and is routinely updated based on observations made with various radars and optical devices. The distribution of objects obtained from this catalog has been used to assess the safety of space traffic now and in the future.[1,2] However, the main information obtained on each object from these observations is the radar scattering cross section, which is not necessarily correlated with its mass.

Although the area-to-mass ratio has been estimated by measuring perturbations of the orbit of debris due to atmospheric drag,[3,4] apparently a more extensive study on the mass and shape of debris is needed. Radar observations at various wavelengths will provide important information on the physical size and shape of the debris. While most tracking radar employ UHF or higher frequencies to obtain a sharp beam and high gain with limited antenna aperture, we demonstrate here that powerful VHF radars also can be used for debris observations.

The middle and upper atmosphere (MU) radar was constructed at Shigaraki, Shiga prefecture, Japan (34.85°N, 136.11°E) in 1984 mainly for the purpose of investigating atmospheric and plasma dynamics in the wide region from the troposphere to the ionosphere.[5]

The radar is a powerful monostatic pulse Doppler radar operating at 46.5 MHz with an active phased-array antenna, which consists of 475 Yagi antennas and identical number of solid-state transmit/receive modules. The design realized a very fast beam steerability. The antenna beam direction can be switched to any direction within the steering range of 30 deg from zenith from pulse to pulse. The antenna aperture is 8330 m^2 (103 m in diam), and the peak and average output power is 1 MW and 50kW, respectively. The antenna beam has a conical shape with the round-trip (two-way) half-power beamwidth of 2.6 deg. The details of the system are described elsewhere.[6,7]

Here we present the experimental setup and preliminary results of a series of observations made with the MU radar as the first attempt of measuring the distributions of orbital debris vs height and scattering cross section at the VHF band.

Observations

The MU radar operates an ionospheric sounding mode about 48 hours every month, measuring the echo power and autocorrelation functions of ionospheric scattered echoes. The same data can be utilized to pick up hard-target echoes from orbiting objects for a height range between 300–1240 km and to determine their statistics. The observations have been made for four beam directions of 20 deg off vertical in the east, west, north, and south directions. For transmission, a 7-bit Barker code with 64-μs subpulses has been used for the power

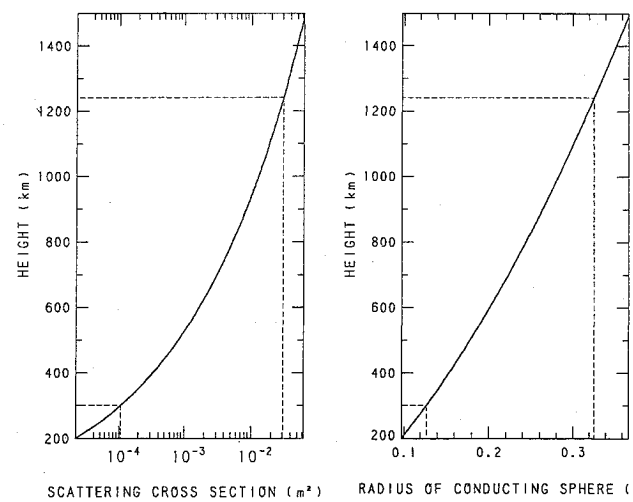

Fig. 1 Detectivity of the MU radar for a hard target in terms of minimum scattering cross section and corresponding radius of perfectly conducting sphere vs height.

Received March 16, 1990; presented as Paper 90-1343 at the AIAA/NASA/DoD Orbital Debris Conference, Baltimore, MD, April 16–19, 1990; revision received Feb. 6, 1991; accepted for publication Feb. 6, 1991.

*Lecturer, Department of Electrical Engineering II.
†Graduate Student, Department of Electrical Engineering II; currently NTT Radio Communication Systems Laboratories, 1-2356 Take Yokosuka-shi, Kanagawa 238-03, Japan.
‡Graduate Student, Department of Electrical Engineering II.
§Professor, Department of Electrical Engineering II.

mode of ionospheric observation. The received echo signals are sampled at 207 different range bins with 4.8-km intervals and averaged over 25 transmitting pulses for incoherent integration. The resultant time resolution is about 1 s.

Figure 1 shows the detectability of the MU radar for a hard target with these parameters in terms of the minimum scattering cross section and corresponding radius of perfectly conducting sphere vs height. The background noise temperature is assumed to be 10,000 K, which is the mean galactic noise temperature at 46.5 MHz. Capability of the MU radar for a hard target is about 1.5×10^{-4} m^2 in its cross section at an altitude of 300 km and about 3.7×10^{-2} m^2 at an altitude of 1240 km, which correspond to radii of conducting spheres of 13 cm and 34 cm, respectively.

As is clear from this figure, most small objects fall within the Rayleigh region of scattering, in which the scattering cross section is much smaller than the physical cross section. While this is an obvious disadvantage in terms of detectivity, a large difference in the operating frequency from other radars usually chosen for this type of study will provide us with a unique opportunity for obtaining the scattering cross section at a much lower frequency.

Data Analysis

These data have shown that in addition to the echoes from the hard targets, there are several other kinds of signals included, such as cosmic noise, incoherent scatter echoes from the ionosphere, and impulsive signals like lightning atmospherics. Also, the observed hard targets include a large number of meteor trails as well as the desired artificial orbiting objects. Ionized trails generated by an encounter of a meteor into the Earth's atmosphere produces strong coherent echoes for the VHF band, which usually last for a fraction of a second. Although their occurrence is limited to a narrow height region of 80–110 km, they are often strong enough to be observed through low-elevation sidelobes of the antenna at much longer ranges.

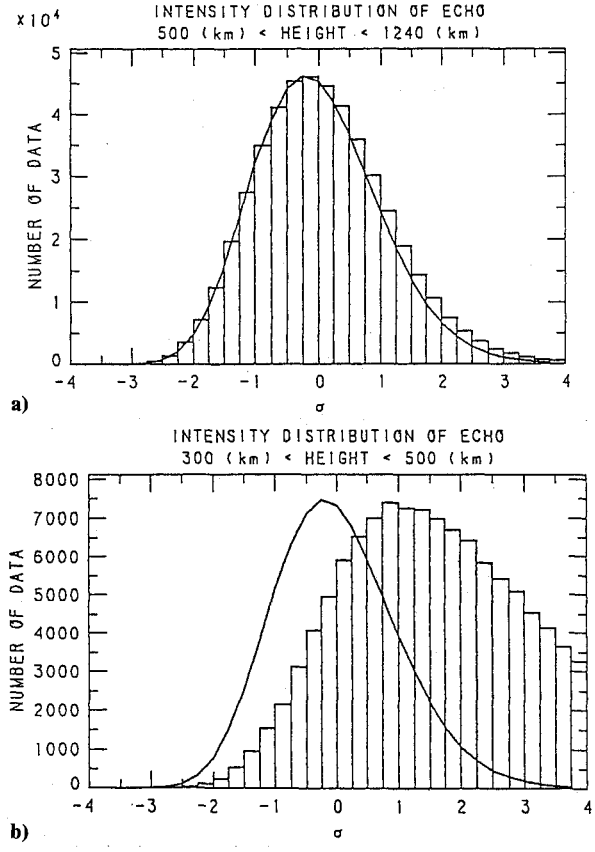

Fig. 2 Intensity distribution of the received power around the mean background noise level. The solid curve shows theoretical χ^2 distribution of the deg 50, and histograms are the data for height regions of a) above 500 km, and b) 300–500 km.

During the MU radar observations, all data are recorded on magnetic tapes in a form of sequential height profiles of the echo power. We have developed an automated algorithm as described below to select echoes from the orbiting objects out of all recorded signals included in the radar echo data. The procedure makes use of the known statistical characteristics of each type of echoes and interferences in classifying them. It consists of two stages: 1) detection of hard targets out of continuous background, and 2) recognition of echoes from desired orbiting objects among other types of signals. The following sections describe some details of the technique.

Detection of Hard Targets

The first step of the data analysis is to detect strong echoes due to hard targets out of continuous background noise. If the noise power was constant, a constant threshold level could be determined with a given false-alarm rate. However, the background cosmic noise level changes with local time and season, and at lower altitudes the ionospheric incoherent scatter echoes, whose magnitude varies both with time and height, add to the background continuum level.

In the following we first describe the process of general data analyses and present the characteristics of background noise and those of the ionospheric incoherent scattering appearing at altitudes lower than 500 km.

In general, signals detected by two-channel (in phase and quadrature phase) receivers of the MU radar constitute real and imaginary parts of the complex baseband signal.

The signal power is calculated by adding the square of these two components. In the case of the cosmic noise, the real and imaginary part are independent random signals that follow a Gaussian distribution. Therefore the power calculated previously follows a χ^2 distribution of the deg 2. To reduce a large fluctuation in a raw data, 25 times of incoherent integration is made to get every 1 s datum at 207 height points for an altitude range from 300 to 1240 km. This averaging process changes the power distribution of the data at each altitude point to a χ^2 distribution of the deg 50.

Actually, at any altitude point above 500 km, the intensity (power) distribution of echoes exactly follows this χ^2 distribution of the deg 50 as shown in Fig. 2a. In such a case, the probability of a signal intensity exceeding seven times the standard deviation (σ) of the previous distribution is estimated to be very small, i.e., about 1.1×10^{-7}. Therefore 7σ is an appropriate value for the threshold level of hard target detection with sufficiently low false-alarm rate against random noise. However, as shown in Fig. 2b, below 500 km of altitude, the intensity distribution of echo does greatly deviate from the χ^2 distribution of the deg 50, due to incoherent scattering echoes from the ionosphere. To remove such an effect, we have to increase the threshold level to 10–15σ.

If we use these larger threshold values for whole altitude range, the minimum detectable cross section of the hard targets is reduced. In our data analyses, we have decided to choose an altitude dependent threshold value that is determined by the following processes. First, the signal level at every altitude is averaged over 2 min and that averaged value is smoothed out by taking a running mean vs height. The threshold level for detecting hard target is determined by

$$P_n' + 7\sigma' \tag{1}$$

This altitude profile depends on local time and season, so that the threshold level is determined individually from real data to be analyzed.

Figure 3a shows an example of an observed time series of the echo power. The solid line denotes the maximum value in each echo power profile consisting of 207 samples. Dashed and dot-dashed lines show mean background noise level and the threshold level, respectively, as described previously.

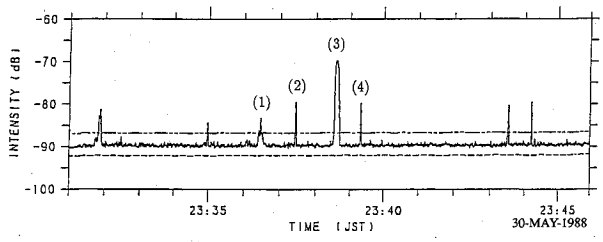

Fig. 3a Example of observed time series of the maximum echo power among each instantaneous height profile.

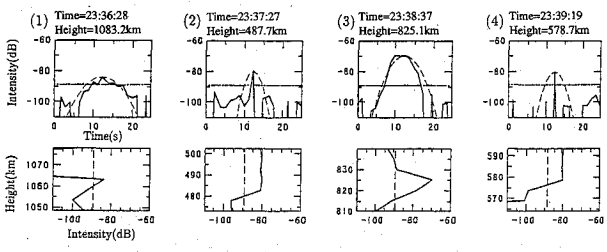

Fig. 3b Height and time profiles around four points that exceed the threshold.

Figure 3b illustrates examples of time and altitude plots of the data around four of the points that exceed the threshold in Fig. 3a. The background noise level that is indicated by a dash-dotted line in the time patterns and by a dashed line in the height patterns is subtracted from these figures. The dashed line in the time pattern illustrates a time sequence of the signal level calculated theoretically from the antenna beam pattern of the MU radar, assuming that the object has a circular orbit. As will be seen later, only cases 1 and 3 are the echoes from orbiting objects. An automated algorithm to discriminate these objects is explained in the following section.

Occasionally, the background signal level is enhanced by 10–20 dB due to the contamination of strong coherent echoes probably originating from the ionospheric field-aligned irregularities due to spread F layers or sporadic E layers. Such periods are removed beforehand manually from the analysis.

Recognition of Echoes from Orbiting Objects

We then examine the time and height patterns of the individual echo. Peculiar time and height patterns accompanied with some kinds of interferences, such as the echoes from overdense meteor trails or external impulsive noises, are used to identify and remove them before examining the echo pattern in details.

Echo Pattern of Orbiting Objects

A small portion of an arbitrary orbit of orbiting objects can be approximated by a circular orbit at the altitude of interest from the point of view of its radial distance vs time of the order of a few tens of seconds. The velocity of a circularly orbiting object is determined by

$$v = \sqrt{G_m/(R_e + H)} \tag{2}$$

The antenna beam pattern of the MU radar $f(\theta)$ is known. In case an orbiting object traverses just over the beam center, the expected echo power should be

$$P_r(t) \propto f(\theta)^2$$

$$\theta = \tan^{-1}[v(t - t_o)/H] \tag{3}$$

where the cross section of the orbiting object is assumed constant. The antenna echo pattern becomes a function of the object altitude only.

To discriminate orbiting objects, the antenna echo patterns thus calculated for the altitudes of the objects are used. Figure 4 illustrates an example of observed echo patterns vs time (s) (solid curve) and theoretically calculated echo pattern (dashed curve). An automated algorithm was developed to identify echoes from orbiting objects by comparing the echo pattern with the theoretical ones using the least squares fitting technique. The conditions for decision were chosen empirically so that the result of the identification matches manual identification.

So far we have assumed that the orbiting objects pass over the antenna main beam. When the target does not pass through the center of the beam, the reduced gain of the beam results in an underestimation of the scattering cross section. If the target passes more than 2 deg off the center of the beam, however, the relative strength of the sidelobes becomes large enough to identify the echo pattern as being multiple peaked. Such echoes are not used in deriving the distribution of orbiting targets shown later, since their scattering cross section cannot be measured accurately. Considering that the measured paths of objects should distribute evenly within 2 deg from the center of the beam, we can calculate the expected magnitude of the underestimate to be about 1.4 dB. The scattering cross section shown in the following sections is compensated for this value.

There are other interesting examples of echoes as shown in Fig. 5, whose intensities violently fluctuate in time. These cases are interpreted as a result of fast spin motions of nonspherical targets. Further analyses of such fluctuations will provide important information on the shape of individual targets.

Echo Pattern of the Meteor Echoes

The meteor trails are generated in the altitude range of 80–110 km, and this trail produces a very strong coherent echo even for low elevation sidelobes of the MU radar, as discussed before. This means that the meteor echo effectively appears as if the echo comes back from the height range of our observations.

The meteor echoes are classified into two types, underdense and overdense echo. While the former has a relatively small electron density at the center of the trail that causes only coherent scattering, the latter is dense enough to cause a total reflection of the radar wave. The former echo lasts only a frac-

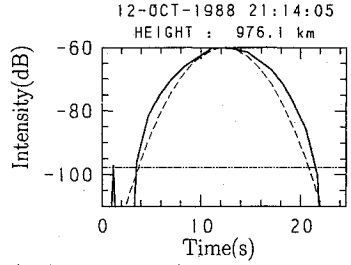

Fig. 4 Example of observed echo pattern vs time (solid curve) and theoretically calculated echo pattern (dashed curve). The dot-dashed line indicates the background noise level, which is subtracted.

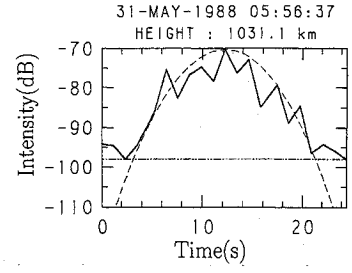

Fig. 5 Example of echo pattern as shown in Fig. 4 but with large fluctuations in the echo power.

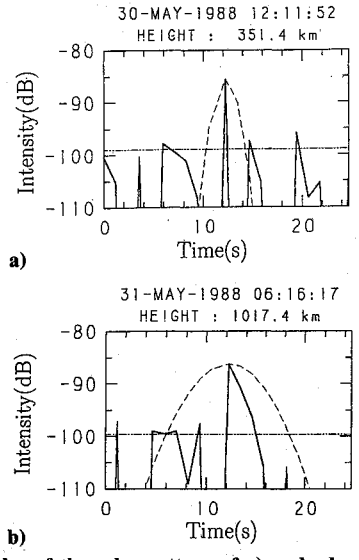

Fig. 6 Examples of the echo pattern of a) underdense, and b) overdense meteor trails.

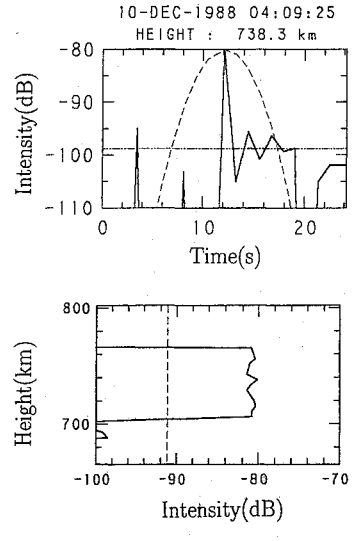

Fig. 7 Example of the time and height patterns of external impulsive noises.

tion of a second, like an impulse, whereas the latter echo builds up sharply within a second and decays slowly with several seconds, as shown in Fig. 6. A characteristic difference of the overdense echoes from the hard target echoes is that the echo shape is asymmetric with respect to the time of the amplitude peak.

Impulsive Noises

The final category of signals exceeding the threshold level for hard-target discrimination is external noises that form sharply isolated impulsive time patterns like the underdense meteor echoes. Most plausible sources of such noise are the lightning atmospherics and artificial discharges due to power switching.

Since we employ the pulse compression technique, echoes from hard targets show an impulsive height pattern only after the decompression operation. In contrast, external impulsive noises have an impulsive height pattern *before* the decompression, so that they show a box-car height pattern of the Barker code itself extending over a height range of 60 km after the cross-correlation operation. Figure 7 shows an example of the time and height pattern due to impulsive noise. These echoes can be identified and removed fairly easily based on this peculiar height pattern.

Percentage of Various Types of Detected Signals

As described above, it has been found that the meteor echoes and impulsive noises are observed in addition to echoes from orbiting objects.

Also, when an orbital object with a large scattering cross section passes through sidelobes of the radar, we get multiple peaks with small intervals in the received time pattern. Although they are interpreted as separate echoes by the automatic selection procedure, they are later recognized as the echo from a single object by checking the intervals between the occurrence of the echoes.

Therefore, many of the signals detected from background based on the threshold determined in the previous section are rejected by these criteria. The percentage of occurrences of various types of signals thus identified are illustrated in Fig. 8 based on the statistics obtained from about 117 h of observations that are examined later. It turns out that the echoes from orbiting objects are only 12.7% of total signals exceeding the threshold level. Only these echoes are used in the statistics that follow.

Statistical Distribution of Orbiting Objects

The previous algorithm has been applied to the MU radar data obtained for a period from May 1988 to January 1989, where during 117 h of observations, a total of 4379 orbiting objects were detected to obtain the distribution of objects with respect to the height and the scattering cross section. Echoes from orbiting objects are detected about once per 2 min.

In spite of all these rejections, a clear sign of contamination due to weak meteor echoes was found in low-altitude data. Figure 9 illustrates the flux, or the number of orbiting objects

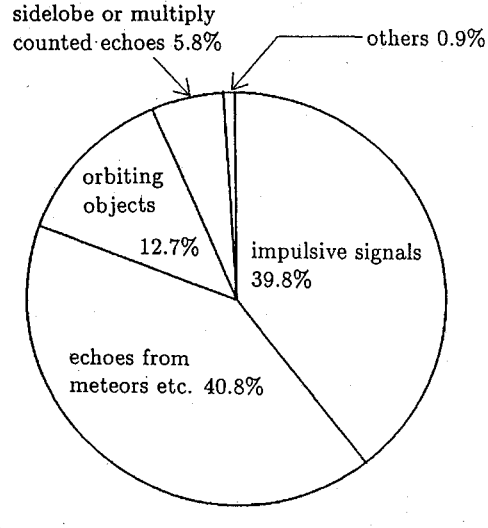

Fig. 8 Percentage of various types of signals classified by the automatic data processing algorithm.

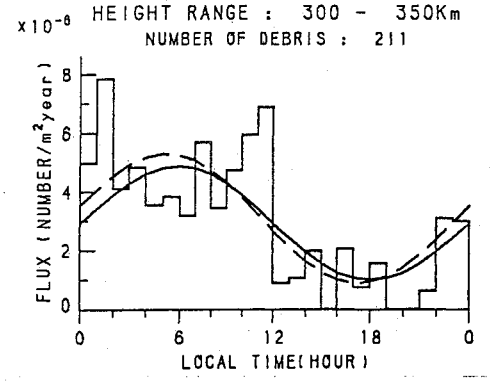

Fig. 9 Example of the local time dependence of the flux of debris at low altitude indicating contamination of weak meteor echoes.

passing through a unit area per year, vs local time of the day (LT) for a height range of 300–350 km. It should be noted that since the present observation is made with a radar having a conical beam, the sample area is its cross section. Thus, the flux shown here times the cross section of a spacecraft target gives the estimated number of impacts on the spacecraft.

A diurnal variation is obvious, as shown by the best fit sinusoids of the 24-h period. The solid curve is a best fit with the time of the maximum fixed to 6 LT, and the dashed curve is obtained without giving constraint on the phase.

It is hard to think of any reason that orbital debris shows such local time dependence because the same object experiences various local time in one orbit, except for those in solar-synchronous orbits. On the other hand, meteor echoes are known to have a clear diurnal variation in their frequency with a maximum at 6 LT and a minimum of almost no occurrence at 18 LT. The magnitude of such diurnal variation decreases with increasing height and becomes negligibly small above 500 km. Also the diurnal variation can be found only in weak echoes with scattering cross sections close to the detection limit. Weak echoes at low altitudes are in fact hard to identify because of their large angular velocity and small margin against statistical fluctuations. At a height of 300 km, for example, only a few samples are available for each target.

Although it is very hard to identify each of these echoes, it is easy to subtract their effect in the obtained distribution. We simply subtract the diurnally varying component from the distribution by taking the minimum value of the fitted sinusoid in Fig. 9 ($= 1.0 \times 10^6$) as the real contribution from orbital debris. It is equivalent to assume that meteor echoes have zero occurrence at 18 LT, which is reasonable as the first-order approximation.

Figure 10 shows the observed height distribution of the orbiting objects after this subtraction for several ranges of the scattering cross section denoted by gray scales. The distribution shows maxima at around heights of 600 km, 800 km, and 1000 km, which agree with those of the distribution calculated by NASA based on the USSPACECOM catalog.[8] The flux is $1\text{–}2 \times 10^{-6}/m^2/yr$ at this height range. Figure 11 draws the same distribution versus the scattering cross section and the diameter of the equivalent conducting sphere. The dashed line denotes the minimum observable cross section at the maximum height of 1240 km. The flux for the cross section smaller than this value is calculated from the data of limited height ranges and thus is less reliable. No correction is applied to compensate for possible height dependence of the size of orbital debris.

In the present study, only the height and cross-sectional distributions measured at 46.5 MHz have been presented without identifying each object. Since the comparison of the radar scattering cross section of the objects at different frequencies will provide useful information on their shape, and hopefully on their mass, an extensive survey with several different wavelengths is strongly needed.

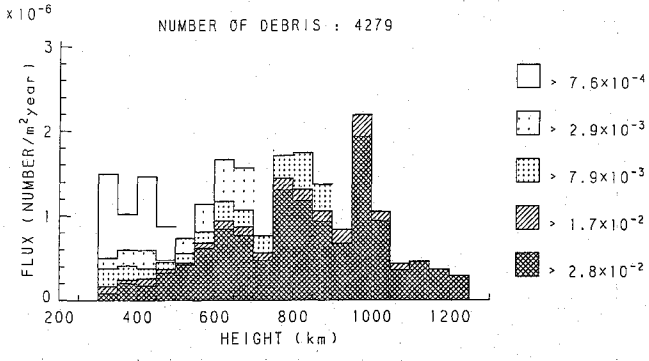

Fig. 10 The observed height distribution of the orbiting objects. The ordinate is expressed in terms of the number of objects passing through a unit area per year. Gray scales indicate the scattering cross section of the objects as shown on the right of the figure.

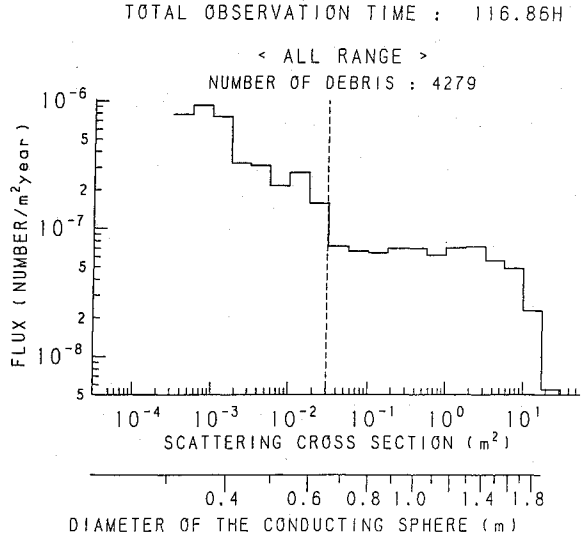

Fig. 11 The flux of orbiting objects vs the scattering cross section. The dashed line denotes the minimum observable cross section at the maximum height of 1,240 km.

Summary

Preliminary results of a series of observations made with the MU radar to determine height distribution of orbital debris were presented as the first attempt at deriving the statistical distribution at VHF. An automatic data processing procedure was first developed to discriminate backscatter echoes from orbiting objects from those of meteors or other interferences. The height distribution of the debris showed good agreement with that obtained from USSPACECOM data using microwave frequency tracking radars and optical telescopes.

The present results have shown that it is feasible to obtain radar scattering cross section of space debris at a frequency of as low as 46.5 MHz. Further observations with the MU radar or similar VHF radars will be an important source of information in studying the relation between the radar cross section and physical characteristics of the debris.

Acknowledgments

The authors wish to thank M. Nagatomo of the Institute of Space and Astronautical Science and H. Matsumoto of the Radio Atmospheric Science Center of Kyoto University for their helpful suggestions and encouragement. They are also grateful to the technical supports for the MU radar experiments by staff members of the Radio Atmospheric Science Center of Kyoto University. Helpful comments and suggestions by reviewers in revising the manuscript are deeply appreciated. The MU radar is owned and operated by the Radio Atmospheric Science Center of Kyoto University.

References

[1]Kessler, D. J., and Cour-Palais, B. G., "Collision Frequency of Artificial Satellites: The Creation of a Debris Belt," *Journal of Geophysical Research,* Vol. 83, June 1978, pp. 2637–2646.

[2]Kessler, D. J., "Sources of Orbital Debris and the Projected Environments for Future Spacecraft," *Journal of Spacecraft and Rockets,* Vol. 18, No. 4, 1981, pp. 357–360.

[3]Badhwar, G. D., Potter, A. D., Anz-Meador, P. D., and Reynolds, R. C., "Characteristics of Satellite Breakups from Radar Cross Section and Plane Change Angle," *Journal of Spacecraft and Rockets,* Vol. 25, No. 6, 1988, pp. 420–426.

[4]Badhwar, G. D., and Anz-Meador, P. D., "Determination of the Area and Mass Distribution of Orbital Debris Fragments," *Earth, Moon, and Planets,* Vol. 45, April 1989, pp. 29–51.

[5]Kato, S., Ogawa, T., Tsuda, T., Sato, T., Kimura, I., and Fukao, S., "The Middle and Upper Atmosphere Radar: First Results Using a Partial System," *Radio Science,* Vol. 19, Nov.-Dec. 1984, pp. 1475–1484.

[6]Fukao, S., Sato, T., Tsuda, T., Kato, S., Wakasugi, K., and Makihira, T., "The MU Radar with an Active Phased Array System: 1. Antenna and Power Amplifiers," *Radio Science,* Vol. 20, Nov.-Dec. 1985, pp. 1155–1168.

[7]Fukao, S., Tsuda, T., Sato, T., Kato, S., Wakasugi, K., and Makihira, T., "The MU Radar with an Active Phased Array System: 2. In-House Equipment," *Radio Science,* Vol. 20, Nov.-Dec. 1985, pp. 1169–1176.

[8]Reynolds, R. C., and Potter, A. E., "Orbital Debris Research at NASA Johnson Space Center, 1986–1988," NASA 102155, Sept. 1989.